time (4–7) are needed to estimate 3000 triplets selected by P_{10} on an IBM 370/158 machine when **k** is allowed to vary over the largest 70 $|E|$'s.

7. Conclusions

The illustrative examples computed by (8) and (10) indicate that these formulas can provide more useful phase information than P_3. The information is of varied sort.

The triplets estimated positive by P_{10}, ranked in a new order of accuracy, define a new convergence map and can actively be used in the tangent procedures. It should also be stressed that the integration of our formulas with the random approaches of phases (Declercq, Germain & Woolfson, 1979) is very easy and can facilitate the convergence from random phases to the correct solution.

The triplets whose cosines are estimated negative by P_{10} often are not sufficiently accurate to be actively used in tangent procedures. However, they can be successfully exploited as a powerful figure of merit for finding out the correct solution in multisolution procedures (Camalli *et al.*, 1984). We stress the point that such a figure of merit is statistically independent of that using negative quartets.

References

BEURSKENS, T., BEURSKENS, G. & VAN DEN HARK, TH. E. M. (1976). *Cryst. Struct. Commun.* **5**, 241–246.

CAMALLI, M., CASCARANO, G., GIACOVAZZO, C., SPAGNA, R. & VITERBO, D. (1984). In preparation.

COCHRAN, W. (1955). *Acta Cryst.* **8**, 473–478.

COLENS, A., DECLERCQ, J. P., GERMAIN, G., PUTZEYS, J. P. & VAN MEERSSCHE, M. (1974). *Cryst. Struct. Commun.* **3**, 119–122.

DECLERCQ, J. P., GERMAIN, G. & WOOLFSON, M. M. (1979). *Acta Cryst.* A**35**, 622–626.

GIACOVAZZO, C. (1977*a*). *Acta Cryst.* A**33**, 527–531.

GIACOVAZZO, C. (1977*b*). *Acta Cryst.* A**33**, 933–944.

GIACOVAZZO, C. (1980). *Direct Methods in Crystallography.* London: Academic Press.

GOLDBERG, I. (1975). *Acta Cryst.* B**31**, 2592–2600.

GOLDBERG, I. & RESMOVITZ, H. (1978). *Acta Cryst.* B**34**, 2894–2896.

HAUPTMAN, H. (1975). *Acta Cryst.* A**31**, 680–687.

HAUPTMAN, H. (1977). Am. Crystallogr. Assoc. Michigan State Meet., 7–12 August 1977. Abstract H3.

HULL, S. E., LEBAN, I., MAIN, P., WHITE, P. S. & WOOLFSON, M. M. (1976). *Acta Cryst.* B**32**, 2374–2381.

SCHENK, H., KOPS, R. T., VAN DER PUTTEN, N. & BODE, J. (1978). *Acta Cryst.* B**34**, 505–507.

SHAKKED, Z. & KENNARD, O. (1977). *Acta Cryst.* B**33**, 516–522.

SUCK, D., MANOR, P. C. & SAENGER, W. (1976). *Acta Cryst.* B**32**, 1727–1737.

VITERBO, D. & WOOLFSON, M. M. (1973). *Acta Cryst.* A**29**, 205–208.

WALLWORK, S. C. & POWELL, H. M. (1980). *J. Chem. Soc. Perkin Trans. 2*, pp. 641–646.

WONG, R. Y. (1978). *Acta Cryst.* B**34**, 3482–3484.

Acta Cryst. (1984). A**40**, 283–291

The Two-Wave X-ray Field Calculated by Means of Integral-Equation Methods

BY JOHANNES BREMER

Division of X-ray Physics and Crystallography, The Norwegian Institute of Technology, The University of Trondheim, 7034 Trondheim-NTH, Norway

(*Received* 10 *March* 1983; *accepted* 15 *December* 1983)

Abstract

The problem of calculating the two-wave X-ray field on the basis of the Takagi–Taupin equations is discussed for the general case of curved lattice planes. A two-dimensional integral equation which incorporates the nature of the incoming radiation, the form of the crystal/vacuum boundary, and the curvature of the structure, is deduced. Analytical solutions for the symmetrical Laue case with incoming plane waves are obtained directly for perfect crystals by means of iteration. The same method permits a simple derivation of the narrow-wave Laue and Bragg cases. Modulated wave fronts are discussed, and it is shown that a cut-off in the width of an incoming plane wave leads to lateral oscillations which are superimposed on the *Pendellösung* fringes. Bragg and Laue shadow fields are obtained. The influence of a non-zero kernel is discussed and a numerical procedure for calculating wave amplitudes in curved crystals is presented.

1. Introduction

One important problem in the theory of X-ray diffraction is to describe wave propagation in general three-dimensional structures which are not crystalline in the traditional sense. It is well known that the Takagi–Taupin method (Takagi, 1969; Taupin, 1964) permits the dynamical X-ray wave-field in both perfect and slightly imperfect crystals to be calculated. A more general way of handling the same problem for statistically distributed defects has recently been put forward by Kato (1980). A variety of situations exists, however,

0108-7673/84/030283-09$01.50

for which the simpler Takagi–Taupin equations are sufficient. Such a case is, for instance, met with in X-ray optics and spectrometry when a crystal is given a well-defined shape through bending with subsequent grinding or etching (Kushnir & Suvorov, 1982; Bremer & Sørum, 1980; Sørum & Bremer, 1980). Precise atomic displacements may be induced also by means of surface films, thermal gradients and dislocations. A limited number of models have been studied analytically by various authors, mainly by means of Riemann-function methods. Takagi's original differential equations have for that purpose been transformed into uncoupled partial differential equations. The effect of a single stacking fault in a perfect crystal has been calculated by Authier & Simon (1968). The exact solution for structures that arise from constant strain gradients has been given by Katagawa & Kato (1974), Litzman & Janáček (1974) and Chukhovskii (1974; Chukhovskii & Petrashen, 1977).

The interaction strength between X-ray photons and crystalline electrons may conveniently be expresssed by means of the complex extinction parameter $\tau_h = \lambda/(\chi_h C)$, where λ is the wavelength, C is the polarization factor and χ_h is the hth Fourier component of the high-frequency susceptibility. Numerical methods (Epelboin, 1977; Nourtier & Taupin, 1981) that are based on approximating the field derivatives by means of finite differences per step length work very well when the steps are much smaller than $|\mathrm{Re}\,(\tau_h)|$. For most crystals $|\mathrm{Re}\,(\tau_h)|$ is typically of order 10^1–10^2 μm. Such parameters as bending radii, crystal thicknesses and wave-front widths are also of macroscopical dimensions and it appears useful to work out iteration procedures where the expansion parameter somehow depends on these length scales. The reason is that a systematic expansion may make it easier to introduce sensible approximation in both numerical and analytical work. The aim of the present paper is to discuss and work out iteration procedures entirely in terms of integral-equation theory. It will also be shown through some examples that the standard dynamical theory of perfect crystals may be obtained in a very simple way.

2. Integral-equation formulation

The solution of the two-wave case will be based on the assumption that each polarization component of the electric field amplitude **D** at an arbitrary position **r** inside the crystals can be written as the eikonal-like sum

$$\mathbf{D}(\mathbf{r}) = \mathbf{D}_0(\mathbf{r}) \exp(-2\pi i \mathbf{k}_0 \mathbf{r}) + \mathbf{D}_h(\mathbf{r}) \exp(-2\pi i \mathbf{k}_h \mathbf{r}), \tag{1}$$

where $\mathbf{k}_0$ and $\mathbf{k}_h (|\mathbf{k}_0| = |\mathbf{k}_h| = 1/\lambda = k)$ refer to the wave vector of the transmitted and diffracted wave, respectively (Fig. 1). The components of the field fulfil Maxwell's equations when (Takagi, 1969; Taupin, 1964)

$$\frac{\partial D_0}{\partial s_0} = -i\pi\tau_{\bar{h}}^{-1} \exp(-2\pi i \mathbf{hu}) D_h, \tag{2}$$

$$\frac{\partial D_h}{\partial s_h} = -i\pi\tau_{\bar{h}}^{-1} \exp(2\pi i \mathbf{hu}) D_0 - 2\pi i k \Delta\theta \sin 2\theta D_h, \tag{3}$$

with $\Delta\theta$ as the deviation from the exact Bragg angle. Polarization effects are included in the definition of τ_h and $\tau_{\bar{h}}$. The oblique coordinates s_0 and s_h are defined in Fig. 1 and the atomic displacement vector $\mathbf{u} = \mathbf{u}(s_0, s_h)$ together with $\Delta\theta$ are given relative to the unstrained crystal. In what follows, effects due to refraction, *average* absorption and unsymmetrical ray paths will be excluded. The transformations

$$D_0 \to D_0 \exp(2\pi i k \Delta\theta \sin 2\theta s_h), \tag{4}$$

$$D_h \to D_h \exp(2\pi i k \Delta\theta \sin 2\theta s_h) \tag{5}$$

allow (2) and (3) to be rewritten in the symmetrical form

$$\frac{\partial D_0}{\partial s_0} = -i\pi\tau_{\bar{h}}^{-1} \exp(-2\pi i \mathbf{hu}) D_h, \tag{6}$$

$$\frac{\partial D_h}{\partial s_h} = -i\pi\tau_{\bar{h}}^{-1} \exp(2\pi i \mathbf{hu}) D_0. \tag{7}$$

Without loss of generality it is now assumed that a natural boundary with coordinates (r_0, r_h) exists at which $D_h(r_0, r_h)$ is zero while $D_0(r_0, r_h)$ is known. In the Laue case, for instance, an obvious choice will be the entrance surface of the crystal, as schematically depicted in Fig. 1. Both phase and amplitude of $D_0(r_0, r_h)$ may vary. At an arbitrary point P inside the semi-infinite crystal the transmitted field is obtained by formally integrating (6) and (7) over the

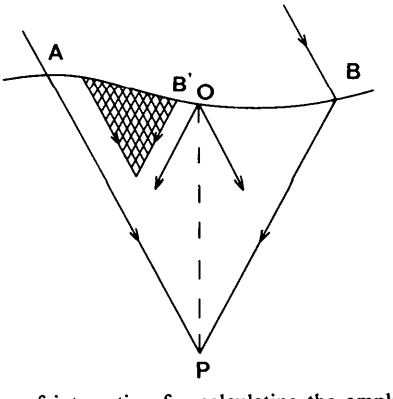

Fig. 1. Area of integration for calculating the amplitude of the transmitted wave in the Laue case. The origin is located at O, and the vectors $\mathbf{k}_0$ and $\mathbf{k}_h$ are parallel to AP and BP, respectively. The unit vectors of the coordinate system are defined by $\mathbf{s}_0 = \mathbf{k}_0/|\mathbf{k}_0|$ and $\mathbf{s}_h = \mathbf{k}_h/|\mathbf{k}_h|$.

variables s_0' and s_h', respectively. The starting points for the two line integrals will be the points A and B' whose coordinates are specified by $r_0 = r_0(s_h)$ and $r_h' = r_h'(s_0')$. When combining the equations and solving for D_0 we get

$$D_0(s_0, s_h) = D_0[r_0(s_h), s_h] - a^{-2} \times \int_{r_0}^{s_0} \int_{r_h'}^{s_h} K(s_h; s_0', s_h') D_0(s_0', s_h')\, \mathrm{d}s_0'\, \mathrm{d}s_h'. \quad (8)$$

The parameter $a = (\tau_h \tau_{\bar{h}})^{1/2}/\pi$ has the dimension of a length and will in what follows play the role of an expansion parameter. Equation (8) is qualitatively a two-dimensional integral equation of the Volterra type. The phase change resulting from the curved lattice planes is expressed by means of the unsymmetrical kernel

$$K(s_h; s_0', s_h') = \exp\{2\pi i \mathbf{h}[\mathbf{u}(s_0', s_h') - \mathbf{u}(s_0', s_h)]\}. \quad (9)$$

This way of calculating the field combines in a single compact expression (8) the three factors which are responsible for the amplitude inside the crystal: (i) the character of the incoming radiation; (ii) the shape of the boundary; (iii) the position of the atoms relative to the unperturbed lattice. The area of validity is the same as for the original Takagi–Taupin equations.

According to (8) the field D_0 at P is given by a phase-modulated integration over D_0 itself inside the area ABP. If the distance from the boundary AB is much less than the extinction length, it is permissible to replace $D_0(s_0', s_h')$ with $D_0(r_0(s_h), s_h]$. By repeating this procedure it is easy to obtain numerical data for arbitrary boundary conditions and (small) atomic displacements. Equation (8) can also be solved (Kanwal, 1971) analytically by replacing $D_0(s_0', s_h')$ inside the double integral with the zeroth-order expansion $D_0^{(0)} = D_0[r_0(s_h), s_h]$ and expanding the amplitude in terms of $(a^{-2})^n$. In doing this we will vary conditions (i) and (iii) above while limiting (ii) to include plane surfaces of semi-infinite crystals. Clearly, since it is the field at the boundary which determines the intensity inside the crystal both the numerical and analytical iteration method will be in agreement with Kirchoff's integral relation. Integral-equation methods have previously been used in dynamical and kinemathical diffraction theory by Afanas'ev & Kohn (1971) and Werner (1974).

3. Solutions for perfect crystals

(a) *Direct solution for incoming plane wave*

In a perfect crystal the displacement $\mathbf{u} = \mathbf{0}$, and the kernel (9) becomes equal to unity. In order to illustrate the use of (8) we now solve directly the Laue case for a plane wave entering a crystal through a plane surface. It is convenient to change to Cartesian coordinates defined by

$$x = (s_h - s_0)\sin\theta, \quad (10)$$

$$y = (s_h + s_0)\cos\theta. \quad (11)$$

The Jacobian is simply equal to $(\sin 2\theta)^{-1}$. With $D_0^{(e)}$ as the constant amplitude for the external vacuum wave, the value for D_0 at the boundary is given by

$$D_0[r_0(s_h), s_h] = D_0^{(e)} \exp[i\delta(x + \alpha y)] \quad (12)$$

according to (4) with $\delta = 2\pi k \Delta\theta \cos\theta$ and $\alpha = \tan\theta$. Equation (8) becomes

$$D_0(x, y) = D_0^{(e)} \exp[i\delta(x + \alpha y)] - a^{-2} \times \int_0^y \mathrm{d}y' \int_{g^{(-)}}^{g^{(+)}} D_0(x', y') \frac{\mathrm{d}x'}{\sin 2\theta}. \quad (13)$$

The area of iteration is a triangle defined by the boundary and the two rays $g^{(\pm)} = x \pm \alpha(y - y')$. The integration over the lateral coordinate x' turns the remaining y' integration into a convolution. With the zeroth-order expansion $D_0^{(o)}(x, y) = D_0^{(e)} \exp[i\delta(x + \alpha y)]$ as the starting value successive iterations yield

$$\begin{aligned} D_0(x, y) = D_0^{(e)}\{&\exp[i\delta(x + \alpha y)] \\ &+ (-2/a^2\delta \sin 2\theta) \exp(i\delta x) \\ &\times \int_0^y \sin[\alpha\delta(y - y_1)] \exp(i\alpha\delta y_1)\, \mathrm{d}y_1 + \ldots \\ &+ (-2/a^2\delta \sin 2\theta)^n \exp(i\delta x) \\ &\times \int_0^y \sin[\alpha\delta(y - y_n)]\, \mathrm{d}y_n \\ &\times \int_0^{y_n} \ldots \int_0^{y_2} \sin[\alpha\delta(y_2 - y_1)] \exp(i\alpha\delta y_1)\, \mathrm{d}y_1 \\ &+ \ldots\}. \end{aligned} \quad (14)$$

A Fourier transformation $T[D_0(x, y)] = \tilde{D}_0(x; q)$ together with the convolution theorem turns (14) into a geometric series which may be summed to give

$$\tilde{D}_0(q) = D_0^{(e)} \exp(-i\alpha\delta y) \times \frac{T[\exp(i\alpha\delta y)]}{1 + 2T[\sin(\alpha\delta y)]/(a^2\delta \sin 2\theta)}, \quad (15)$$

after correcting for the phase transformation (4). Equation (15) is simply the Fourier transform of the *Pendellösung*. Using the condition $D_0(y) = 0$ for $y < 0$ and substituting $T[\exp(-\varepsilon y + i\beta y)] = i/(q + \beta + i\varepsilon)$ we find

$$\tilde{D}_0(q) = D_0^{(e)} \tfrac{1}{2} i \exp(-i\alpha\delta y) \times \left[\frac{1 + \tanh\nu}{q + \cosh\nu/(a\cos\theta)} + \frac{1 - \tanh\nu}{q - \cosh\nu/(a\cos\theta)}\right], \quad (16)$$

after introducing $w = \sinh\nu = \Delta\theta \sin 2\theta/(\chi_h\chi_{\bar{h}})^{1/2}$

and letting $\varepsilon \to 0$. With $S_{0(h)} = y/(a\cos\theta)$ and (2) we arrive at

$$D_0(S_0) = D_0^{(e)} \frac{\cos(S_0 \cosh\nu - i\nu)}{\cosh\nu} \exp(-iS_0 \sinh\nu), \tag{17}$$

$$D_h(s_h) = -iD_0^{(e)} \times \left(\frac{\chi_h}{\chi_{\bar{h}}}\right)^{1/2} \frac{\sin(S_h \cosh\nu)}{\cosh\nu} \exp(-iS_h \sinh\nu). \tag{18}$$

Equation (18) could have been obtained directly by deducing and solving an analogous integral equation for D_h. The steps leading up to (17) and (18) show the feasibility of solving (8) through iteration. The area of validity for both (17) and (18) is restricted to monochromatic waves with constant amplitudes and wave vectors.

(*b*) *Wave-front-modulated Laue case*

Writing $D_0^{(e)} = D_0^{(e)}(r_0, r_h)$ in order to allow for non-constant wave fronts we now discuss the corresponding crystal fields. Although variations of the type $D_0^{(e)} \propto \exp(cs_h)$, with c generally complex, easily may be incorporated in (12), (17) and (18), we will work out an alternative method. The simplest kind of wave-front modulation occurs when a cut-off is imposed on the width of the X-ray bundle by means of a slit system. Diffraction effects caused by the slit edges themselves will not be treated here. Another type of deviation from the plane-wave case is met with when the direction of $\mathbf{k}_0$ is not constant. This may happen for instance when a point source emitting spherical waves is located sufficiently close to the crystal. However, constructive interference for the diffracted wave requires that the corresponding variation in $\Delta\theta$ must be of small order. This ensures that the slight rotation of the coordinate system of Fig. 1 may be ignored for most practical crystal dimensions.

The solutions (17) and (18) will be found to be valid for shallow depths y when the wave-front width exceeds the slit width $2d$. Decreasing d will finally lead to the following. (i) A replacement of the 'triangular' area of integration in Fig. 1 with the cross-hatched area shown in Fig. 2. This follows immediately from a consideration of the lower integration limits in the two integrals leading from (6), (7) to (8). (ii) Introduction of transverse Fourier components for the wave vector. It is convenient to discuss these effects according to whether the front width is much smaller than, or of the same order as, the extinction length. When $d \ll |\mathrm{Re}(\tau_h)|$ we may put the incoming wave directly equal to $D_0^{(e)}\delta(s_\perp)$ with $s_\perp = s_h \sin 2\theta$. The iteration area takes the form of a parallelogram since $r_0 = r_h = 0$. A straight-forward iteration of (8) yields

$$D_0(s_0, s_h) = \frac{D_0^{(e)}}{\sin 2\theta}\left[\delta(s_h) \exp(2\pi ik\,\Delta\theta s_h \sin 2\theta) + \left(\frac{-1}{a^2}\right)s_0 + \ldots + \left(\frac{-1}{a^2}\right)^n \frac{s_0^n s_h^{n-1}}{n!(n-1)!} + \ldots\right] \times \exp(-2\pi ik\,\Delta\theta s_h \sin 2\theta), \tag{19}$$

where both $D^{(e)}$ and $\Delta\theta$ have their 'local' values at $s_0 = s_h = 0$. Using the relationship $z\partial J_\nu(z)/\partial z = zJ_{\nu-1}(z) - \nu J_\nu(z)$ for Bessel functions of integer order ν, (19) and (2) give

$$D_0(s_0, s_h) = \frac{-D_0^{(e)}}{a\sin 2\theta}\left(\frac{s_0}{s_h}\right)^{1/2} J_1\left[\frac{2}{a}(s_0 s_h)^{1/2}\right] \times \exp(-2\pi ik\,\Delta\theta s_h \sin 2\theta) \tag{20}$$

$$D_h(s_0, s_h) = \frac{-iD_0^{(e)}}{a\sin 2\theta}\left(\frac{\chi_h}{\chi_{\bar{h}}}\right)^{1/2} J_0\left[\frac{2}{a}(s_0 s_h)^{1/2}\right] \times \exp(-2\pi ik\,\Delta\theta s_h \sin 2\theta) \tag{21}$$

when excluding the exciting wave. The agreement between the fringe pattern (20), (21) and the 'spherical-wave' theory of Kato (1974) is due to the small angle of acceptance for the incoming wave or – equivalently – the small width of the diffraction curve for a perfect crystal. The above derivation involves only a simple iteration (19) of (8) and is for that reason considerably simpler than the Riemann function method.

The $d \gtrsim |\mathrm{Re}(\tau_h)|$ case may be solved by rewriting (19) for a general wave location s_h' and integrating out the corresponding lateral coordinate x'. It is convenient to substitute $u = (x - x')/\alpha y$ and express the result in terms of S_h defined as in (18). We find, in agreement with calculations (see for instance Authier & Simon, 1968) based on formulating partial

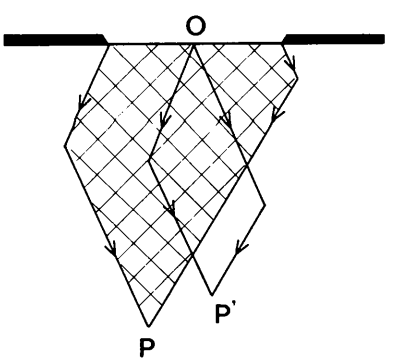

Fig. 2. Effect of limiting the width of the incoming wave front (cross-hatched region). The parallelogram defined by O and P' illustrates the $d \ll |\mathrm{Re}(\tau_h)|$ case.

differential equations for the field,

$$D_h(S_h; f_1, f_2) = \frac{-i}{2} S_h \left(\frac{\chi_h}{\chi_{\bar{h}}}\right)^{1/2} \int_{f_2}^{f_1} D_0^{(e)}(u) \times J_0[S_h(1-u^2)^{1/2}] \exp[-i\Phi(u)]\, du. \quad (22)$$

Here $f_2 = (x-d)/\alpha y$, $f_1 = (x+d)/\alpha y$, and the origin is located in the middle of the slit. When $|x \pm d| \geq \alpha y$ the integration limits reach their maximal values $f_{1,2} = \pm 1$. The phase is given by

$$\Phi(u) = S_h w(1 \pm u), \quad (23)$$

where in the most general case w itself may be a function of u, and the upper sign is to be used for Laue diffraction. The lower sign will be discussed later.

The ideal case of a semi-infinite incoming 'plane' wave with a constant amplitude is shown schematically in Fig. 3(*a*). Such a wave form is useful as a first step in understanding the effect of illuminating the crystal with non-planar waves. In the region to the right of the line AP both the diffracted and the transmitted field must vanish, and the usual *Pendellösung* has to be valid to the left of AP'. This follows from the derivation of (8) or – alternatively – a consideration of those waves that are able to reach the point in question after an arbitrary number of scattering events (Kato, 1974). The field in the half-shadow region PAP' has to be continuous across AP and AP'. Choosing A as origin for x allows us to put $f = f_1 = x/\alpha y$ and $f_2 = -1$ in (22). The resulting integral is tabulated (Gradshteyn & Ryzhik, 1980) for $f = 0$. Expressing the Bessel function in terms of u by using binomial expansions we get

$$D_h(S_h; f) = \frac{-i}{2} D_0^{(e)} \left(\frac{\chi_h}{\chi_{\bar{h}}}\right)^{1/2} \times \left[\sin S_h + S_h \int_0^f \sum_{p=0}^{\infty} \sum_{k=0}^{p} \left(\frac{iS_h}{2}\right)^{2p} \frac{(-u^2)^k\, du}{p!\,k!\,(p-k)!}\right] \quad (24)$$

for $\Delta\theta = 0$. Instead of performing this double summation diagonally we sum each 'column' separately and obtain an infinite series of Bessel functions of order n, *i.e.*

$$D_h(S_h; f) = \frac{-i}{2} D_0^{(e)} \left(\frac{\chi_h}{\chi_{\bar{h}}}\right)^{1/2} \times \left[\sin S_h + S_h f \sum_{n=0}^{\infty} \left(\frac{S_h}{2} f^2\right)^n \frac{J_n(S_h)}{n!(2n+1)}\right] \quad (25)$$

after integration. It turns out that only the first few orders of n give a significant contribution to the amplitude. In the region to the right of A, $f \leq 0$ and equation (25), which may be looked upon as a 'generalized' pendulum solution, is therefore automatically valid for the whole half-shadow area. Continuity of the field is ensured since it can readily be shown that the sum over n will always reduce to an expansion of $\pm \sin S_h$ when $f = \pm 1.0$. This will exactly compensate for the sinusoidal oscillation along the ray AP ($x = -\alpha y$) while doubling its amplitude along AP' ($x = \alpha y$). A numerical evaluation of $I(S_h; f) = |D_h(S_h; f)|^2$ is shown in Fig. 3(*a*) and verifies this conclusion. It also serves to illustrate that the strength of the *Pendellösung* has fallen to exactly 50% of its normal value when $x = 0$. Exhibited in Fig. 3(*a*) is an additional lateral oscillation. It is important to note that this effect is due only to the limitation of the wave-front width. Fig. 3(*b*) displays the fringe pattern predicted by (25) when using two slit edges. Because

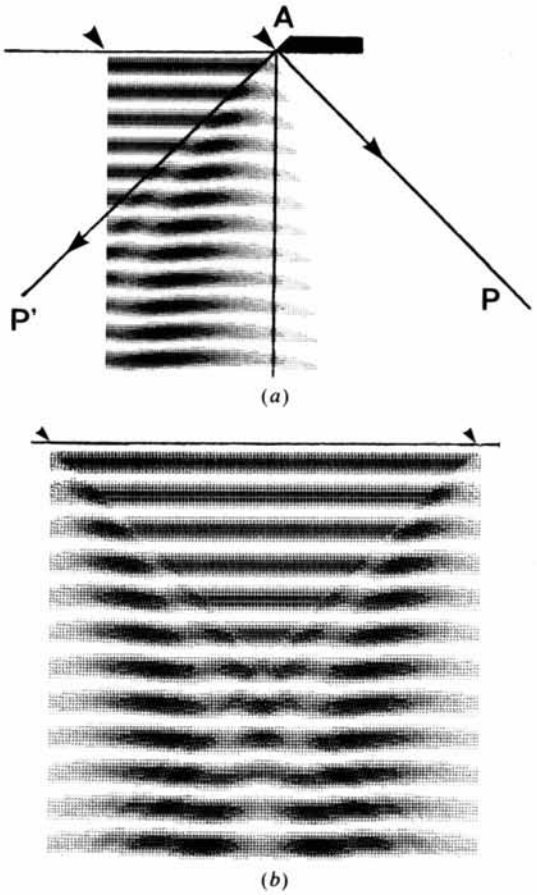

Fig. 3. Symmetrical Laue diffraction ($\Delta\theta = 0$). (*a*) Boundary conditions approximated by semi-infinite 'plane' wave with cut-off at A. The pendulum solution to the left goes continuously into the shadow field along AP' and vanishes completely at AP. The field is generally non-zero inside the whole area $P'AP$ but is not visible near AP for technical reasons. (*b*) Two Laue shadow fields (to the left and right) and their superposition (lower middle region) excited by a rectangular wave-front shape. (See text.)

of the definition of the parameter f the field structure in Fig. 3(a) will be symmetrically present at both sides of the incoming wave. Near the boundary it is always possible to have $f_{1,2}=\pm 1$, and a conventional pendulum solution field will therefore be set up there, as shown in the upper middle region of Fig. 3(b). If we evaluate f_1 and f_2 in (22) for the area below this region we find that we have to add together two equations of the type (25), each with its own value for f. The oscillatory structure that arises from this superposition is seen to have a hyperbolical shape. The distance between the top point of the hyperbolical pattern and the boundary decreases when d goes towards zero, leading to a gradual obliteration of the shadow field to the left and right and the pendulum solution in the middle. Using (25) it is thus possible to give a description of the intensity fringes irrespectively of whether $d>|\mathrm{Re}\,(\tau_h)|$, $d\simeq|\mathrm{Re}\,(\tau_h)|$ or $d<|\mathrm{Re}\,(\tau_h)|$. This is in strong contrast to (21) which ceases to be valid for wide wave fronts. The validity of Fig. 3(b) is based on the assumption of a rectangular shape for the wave front. Such a profile leads to difficulties when attempting to solve (2), (3) numerically (Authier, Malgrange & Tournarie, 1968). When intercepting a plane incoming wave with the aid of a slit, Fresnel effects will cause the boundary conditions for the crystal field $\{D_0[r_0(s_h), s_h]$ in (8)$\}$ to depend also on the distance between the crystal and the slit. Although exhibiting a somewhat irregular shape, the calculated intensity distribution of Authier *et al.* (1968) has been interpreted as a kind of angular amplification of the X-ray field by the crystal.

Since D_h given by (25) is continuous across the lines AP and AP' in Fig. 3(a) both field and intensity will be continuous at the various border lines of Fig. 3(b). The only effect of the assumed vertical flanks of the incoming wave is to make the gradient of the field discontinuous. These discontinuities will be of no concern here. Equations (2), (3) and (8) will respond correctly to field variations that occur over lateral distances comparable in scale to the extinction length.

(*c*) *Wave-front modulated Bragg case*

A narrow-wave Bragg field that is analogous to (20), (21) was, to the author's knowledge, first derived by Uragami (1969). Starting with (8) we will now obtain the field expressions with the help of the iteration procedure used in deriving (20), (21). In addition, we will calculate the field excited inside the crystal by a plane wave, and the effect of limiting the width will thereafter be considered (semi-infinite case). As follows from the derivation of (8) the iterations have to take place over the cross-hatched area of Fig. 4 when the incoming ray bundle is infinitely narrow. The diffracted-wave amplitude is zero along AP while the transmitted amplitude vanishes at the crystal surface except the entrance point A. Waves that are re-scattered above the iteration area are automatically included. Substituting $r_0=s_h$ and $r_h=0$ in (8) gives immediately upon iteration

$$D_0(s_0, s_h)=\frac{D_0^{(e)}}{\sin 2\theta}\Big[\delta(s_h)\exp(2\pi iks_h\,\Delta\theta\sin 2\theta) + \frac{-1}{a^2}(s_0-s_h)+\ldots + \left(\frac{-1}{a^2}\right)^n\frac{1}{n!(n-1)!} \times(s_0^n s_h^{n-1}-s_h^n s_0^{n-1})+\ldots\Big] \times\exp(-2\pi ik\,\Delta\theta\, s_h\sin 2\theta), \tag{26}$$

when using the coordinate system of Fig. 4. Excluding the exciting wave itself we get

$$D_0(s_0, s_h)=\frac{D_0^{(e)}}{a\sin 2\theta}\left[\left(\frac{s_h}{s_0}\right)^{1/2}-\left(\frac{s_0}{s_h}\right)^{1/2}\right] \times J_1\left[\frac{2}{a}(s_0s_h)^{1/2}\right]\exp(-2\pi ik\,\Delta\theta\, s_h\sin 2\theta), \tag{27}$$

$$D_h(s_0, s_h)=\frac{-iD_0^{(e)}}{a\sin 2\theta}\left(\frac{\chi_h}{\chi_{\bar h}}\right)^{1/2}\left\{J_0\left[\frac{2}{a}(s_0s_h)^{1/2}\right] + \frac{s_h}{s_0}J_2\left[\frac{2}{a}(s_0s_h)^{1/2}\right]\right\} \times\exp(-2\pi ik\,\Delta\theta s_h\sin 2\theta), \tag{28}$$

where the latter expression is calculated by means of (6).

In order to calculate the field arising from an extended wave front we define

$$x=-(s_0+s_h)\cos\theta, \tag{29}$$

$$y=(s_0-s_h)\sin\theta \tag{30}$$

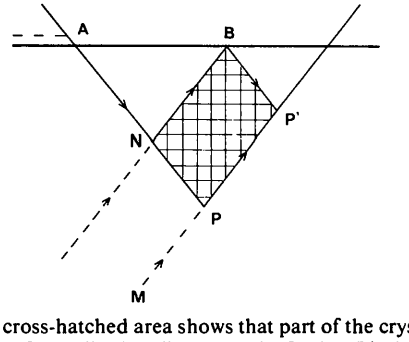

Fig. 4. The cross-hatched area shows that part of the crystal which is capable of contributing directly to the field at P' when excited by a narrow wave at A. Re-scattered waves within the non-hatched triangle ABN must eventually enter the iteration area in order to reach P' and are therefore also included. The origin is located at A and the unit vectors $\mathbf{s}_0$ and $\mathbf{s}_h$ are parallel to AN and NB, respectively.

and allow both the amplitude and the phase to vary along the surface. In contrast to the narrow-front case the entire part of the crystal lying to the left of the broken line MP' is able to propagate and rescatter waves towards P' – granted a wide enough front width. In practice, howevever, contributions from layers lying deeper than the extinction distance will vanish. From (28)

$$D_h(S_h; f_1, f_2) = \frac{-iS_h}{2}\left(\frac{\chi_h}{\chi_{\bar{h}}}\right)^{1/2} \int_{f_1}^{f_2} D_0^{(e)}(u) \times \left\{ J_0[S_h(u^2-1)^{1/2}] + \frac{u-1}{u+1} \times J_2[S_h(u^2-1)^{1/2}] \right\} \exp[i\Phi(u)]\, du, \tag{31}$$

with integration limits determined by the slit system and $u = (x'-x)\alpha/y$. Since S_h is proportional to the distance from the surface along the reflected ray and the Bragg and Laue angles are complementary, the definitions of Φ and S_h may be kept unmodified when using the lower sign in (23). For a plane wave we substitute the values $f_1 = 1$ and $f_2 = \infty$. Using tabulated values for the integrals we arrive at

$$D_h(S_h) = D_0^{(e)}\left(\frac{\chi_h}{\chi_{\bar{h}}}\right)^{1/2} \exp[S_h(iw - (1-w^2)^{1/2}] \times [w - i(1-w^2)^{1/2}] \tag{32}$$

whose value at the surface ($S_h = 0$) is in agreement with the expression given by Uragami (1969) when choosing the physically correct sign for the square roots inside the parentheses. Another special case of (31) is represented by a cut-off in the width of a plane wave. In contrast to the analogous Laue case we want to find the field at the surface. The amplitude distribution across the reflected beam along the x direction may be obtained by using $u \gg 1$ in (31). The necessary integrals are tabulated (Gradshteyn & Ryzhik, 1980), giving

$$D_h(x) = -iD_0^{(e)}\left(\frac{\chi_h}{\chi_{\bar{h}}}\right)^{1/2} \times \left[2\sum_{n=0}^{\infty} J_{2n+1}\left(\frac{x}{a\cos\theta}\right) - J_1\left(\frac{x}{a\cos\theta}\right)\right] \tag{33}$$

for a simple slit edge located at A (Fig. 4). The origin for x is A. The presence of straight-edge diffraction in air is neglected and $\Delta\theta = 0$. When $x \gg |\mathrm{Re}\,(\tau_h)|$ the first term inside the parentheses approaches unity while the contribution from J_1 can be neglected. There is agreement between (32) and (33) since $w = 0$ in the middle of the Bragg total-reflection range and S_h is defined to be zero at and above the crystal surface. The shadow field (33) will be of importance when x is of the same order as the extinction length. In practice, only the first few orders n will contribute – as in the transmission case.

4. Non-zero kernel

Excluding the trivial case of constant displacements we now allow the kernel (9) to be a function of s_0 and s_h. Without loss of generality we redefine the Laue angle so that $\mathbf{u}(0, 0) = \mathbf{0}$. Alternatively, the crystal planes may be made to curve in such a manner that the atoms near the origin remain unshifted. The displacement field is split into three parts as follows;

$$\mathbf{u}(s_0, s_h) = \mathbf{u}_0(s_0) + \mathbf{u}_h(s_h) + \mathbf{u}_{0h}(s_0, s_h). \tag{34}$$

Such a division is useful since expanding $\mathbf{u}(s_0, s_h)$ around $\mathbf{u}(0, 0)$ in terms of s_0 and s_h will, for instance, cause $\mathbf{u}_{0h}$ to take care of the cross terms between the partial derivatives. As a first step we discuss in this paper the modifications of the integral equation methods when $\mathbf{u}_0 \neq \mathbf{0}$ and $\mathbf{u}_h \neq \mathbf{0}$.

According to (9) any contribution from $\mathbf{u}_0(s_0)$ will be subtracted away. Within the area of validity for the Takagi equations the intensity pattern will therefore not be influenced at all by this deformation class. One of the earliest discussions of phenomena of this kind was given by Penning & Polder (1961). In order to illustrate the effect for the Laue case, the atomic planes of the perfect crystal in Fig. 5 are shown before (unbroken lines) and after (broken lines) the action of a displacement $\mathbf{hu}_0 \propto s_0^3$. In the unperturbed lattice an arbitrary atom located at P will be hit by both multiply scattered D_0 and D_h waves. In a strained crystal, however, both lattice parameter d and angle of entrance θ will vary along an arbitrary ray path because of the non-parallel planes. The conditions for having constructive interference, as expressed through Bragg's law, are therefore no longer fulfilled.

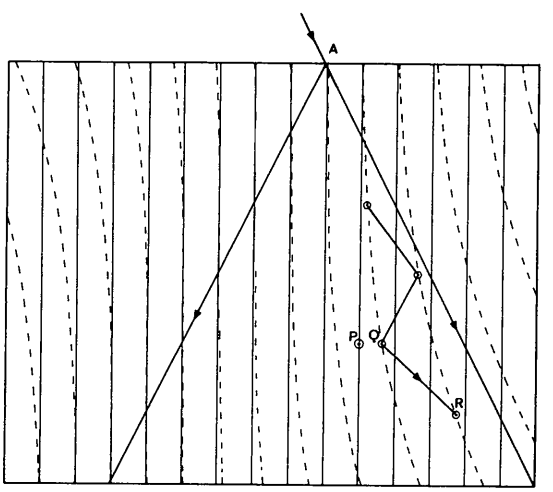

Fig. 5. Crystal planes shown before (unbroken lines) and after (broken lines) the action of the displacement field $\mathbf{hu} \propto s_0^3$. (See text.)

One exception, however, must be wave propagation in the $\mathbf{s}_0$ and $\mathbf{s}_h$ directions. The atom originally located at P has Q as its new position and the change in d when going from Q to R is given by (Fig. 5)

$$\Delta d \simeq \frac{1}{2}\frac{\partial|\mathbf{u}_0|}{\partial s_0}\Delta s_0, \tag{35}$$

where Δs_0 is the distance QR. This increment is exactly compensated by the smaller angle of entrance

$$\Delta\theta \simeq -\frac{1}{2}\left(\frac{\partial|\mathbf{u}_0|}{\partial s_0}\Delta s_0\right)/(d/\tan\theta), \tag{36}$$

giving $\Delta\theta = -\Delta d/d\tan\theta$, which is in agreement with a differentiation of Bragg's law. Multiple scattering and photoelectric absorption will therefore take place as in the unstrained crystal, leaving amplitude, phase and intensity as before. This conclusion remains valid for all incoming 'plane'-wave widths. In contrast, the influence of a displacement field $\mathbf{u}_h(s_h)$ on amplitude and intensity will vanish only for an extremely narrow wave front, and new phases will be introduced even in this case. An impression of this situation may be obtained by reversing the roles played by $\mathbf{s}_0$ and $\mathbf{s}_h$ in Fig. 5. When the kernel (9) takes the form

$$K(s_h; s_h') = \exp\{2\pi i\mathbf{h}[\mathbf{u}_h(s_h') - \mathbf{u}_h(s_h)]\}, \tag{37}$$

the earlier solutions (20) and (21) have to be multiplied by $\exp[-2\pi i\mathbf{h}\mathbf{u}_h(s_h)]$ in order to be valid. This follows immediately from an iteration of (8) when using (37) together with a δ function for the incoming rays. Equations (22), (23) are valid for extended wave fronts when redefining Φ in (23) to including this additional phase.

One of the simplest classes of non-crystallographic lattices is represented by planes fanning out from a common (fictitious) point. Such a structure may arise locally for a slowly changing curvature resulting, for instance, from elastic bending. We assume that the convergence of the planes is perfect, and that the convergence point is located at a distance R above the crystal. The X-rays enter the crystal from above and a plane surface is assumed. In the Laue case a fan-shaped lattice system may be described by means of the (horizontal) displacement vector $u_x = \mathbf{u}\cdot\mathbf{x}/|\mathbf{x}| \simeq xy/R$. Therefore, the phase correction according to (10), (11) must take the form $-i\pi s_h^2 \sin 2\theta/Rd$. When including this in (23) we get

$$\Phi'(u) = \Phi(u) + \frac{\pi}{\lambda R}\left[\frac{(y\sin\theta)^2}{\cos\theta}(1-u^2) + 2xy(1+u)\sin\theta\right]. \tag{38}$$

As $R\to\infty$ the orientation of the planes will become increasingly parallel and the intensity pattern will pass continuously into the fringe system of a perfect crystal. For small depths and a finite R we may neglect the second-order term in (38) and, using $\Delta'\theta = \Delta\theta + x/R$ instead of $\Delta\theta$, one finds that Φ' will be of the same form as Φ. The meaning of this is that local pendulum solutions (18) with extinction distances depending on the lateral coordinate x and the degree of fanning of the planes are set up. $\Phi'(u)$ will oscillate more rapidly than the Bessel function at depths $y \gg R\lambda/(|\mathrm{Re}\,(\tau_h)|\sin^2\theta)$ and will have an extreme value at $u = (x + R\,\Delta\theta)/\alpha y$. The integral (22) can therefore be evaluated by the method of stationary phase when $|x + R\,\Delta\theta| \le \alpha y$. We get

$$D_h(s_0, s_h) \propto \frac{(\lambda R)^{1/2}}{a} J_0\left[\frac{2}{a}(s_0 s_h)^{1/2}\right] \tag{39}$$

when locating the origin at the point where $\Delta\theta = 0$ and excluding the phase. The corresponding intensity distribution has therefore an angular behaviour which is identical to the fringe system excited by a point source on the surface of a perfect crystal.

Numerical solutions capable of dealing with both the $\mathbf{u}_h$ and $\mathbf{u}_{0h}$ terms may be obtained in two principally different ways. (i) A direct numerical iteration of (8) is able to give simultaneously better values for every point lying inside the iteration area. The quality of a solution of this kind will decrease when increasing the distance from the boundary. (ii) Another method consists of the phase change (4) with successive numerical integrations of (6) and (7) along $\mathbf{s}_0$ and $\mathbf{s}_h$. The effect of a deviation $\Delta\theta$ from the Bragg condition is now economically expressed through the boundary conditions. The two (symmetrical) equations may be rewritten as

$$\begin{bmatrix} 1 & -A_{mn}^{\bar{h}} \\ -A_{mn}^{h} & 1 \end{bmatrix}\begin{bmatrix} D_{mn}^{0} \\ D_{mn}^{h} \end{bmatrix} = \begin{bmatrix} (D_{m-1,n}^{0} + A_{m-1,n}^{\bar{h}} D_{m-1,n}^{h}) \\ (D_{m-1,n+1}^{h} + A_{m-1,n+1}^{h} D_{m-1,n+1}^{0}) \end{bmatrix} \tag{40}$$

when the integration length Δ is small. The upper bound for Δ is to be judged from $|\mathrm{Re}\,(\tau_h)|$ or the smallest distance over which significant changes in $\mathbf{hu}$ occur, and $A_{mn}^{h} = -i\pi\Delta\exp(2\pi i\mathbf{hu})/2\tau_h$. The subscripts m and n are proportional to depth and lateral distance, respectively. The product $m\Delta$ is equal to the distance from the surface along the incoming ray to just that mesh point (m, n), where $D_0 = D_{mn}^{0}$ and $D_h = D_{mn}^{h}$. As an example the calculated intensity distribution for a bent Si crystal is reproduced in Fig. 6. These simulations have been performed for the symmetrical Laue case with an incoming plane wave. Other parameters include, $R = 20$ m, $\theta = 10{\cdot}6°$, $\lambda = 0{\cdot}709$ Å, and $|\mathrm{Re}\,(\tau_h)| = 36$ μm. The fringe system is in agreement with the behaviour to be expected from the discussion of the $\mathbf{u}_0$ and $\mathbf{u}_h$ terms for small depths. Not shown in Fig. 6 is the complicated structure in the medium y region and the simpler hyperbolical pattern (39) at larger y.

5. Concluding remarks

The systematic application of integral-equation theory has permitted straight-forward derivations of analytical expressions for the field generated by two coupled waves. Furthermore, the method has the advantage of being easily accessible to a physical interpretation. When an X-ray wave is transmitted over a small distance inside a crystal the probability for a single scattering event is much higher than the probability for double scattering, triple scattering and so on. The basis for the utility of the numerical method (40) is therefore that the successive layers in the crystal are chosen so close together that the probability for multiple reflection can be neglected. Since being over s_h and s_0, however, the two integrals must be proportional to the probability for scattering and re-scattering, respectively. This must mean that a general term of nth order in any of the analytical iteration procedures has to be identical with the contribution from waves that are scattered and re-scattered n times. So far, the influence of average absorption, asymmetrical reflections, and coupling of three or more waves has been neglected. In many circumstances, for instance spectrometry, these factors are either trivial or unimportant. Complicated phenomena such as, for instance, diffraction focusing require that effects due to crystal shape and refraction are considered for the various classes of incoming wave packets.

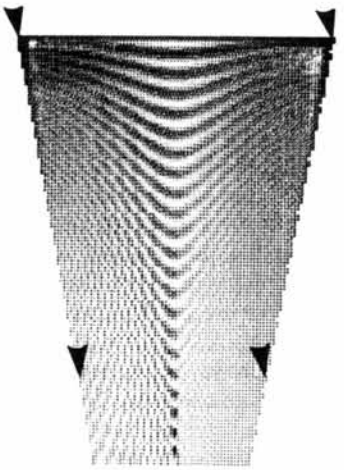

Fig. 6. The intensity of the transmitted wave as calculated from the numerical solution (40) of two coupled integral equations for the field. Fanning planes, not shown, converge above the crystal with $R = 20$ m. The arrows point in the direction of the incoming plane wave. (See text).)

References

AFANAS'EV, A. M. & KOHN, V. G. (1971). *Acta Cryst.* **A27**, 421–430.

AUTHIER, A., MALGRANGE, C. & TOURNARIE, M. (1968). *Acta Cryst.* **A24**, 126–136.

AUTHIER, A. & SIMON, D. (1968). *Acta Cryst.* **A24**, 517–526.

BREMER, J. & SØRUM, H. (1980). *J. Appl. Cryst.* **13**, 354–358.

CHUKHOVSKII, F. N. (1974). *Kristallografia*, **19**, 482–488.

CHUKHOVSKII, F. N. & PETRASHEN, P. V. (1977). *Acta Cryst.* **A33**, 311–319.

EPELBOIN, Y. (1977). *Acta Cryst.* **A33**, 758–767.

GRADSHTEYN, I. S. & RYZHIK, I. M. (1980). *Table of Integrals, Series and Products.* New York: Academic Press.

KANWAL, R. P. (1971). *Linear Integral Equations.* New York: Academic Press.

KATAGAWA, T. & KATO, N. (1974). *Acta Cryst.* **A30**, 830–836.

KATO, N. (1974). In *X-ray Diffraction*, edited by L. V. AZÁROFF, pp. 176–438. New York: McGraw-Hill.

KATO, N. (1980). *Acta Cryst.* **A36**, 763–769.

KUSHNIR, V. I. & SUVOROV, E. V. (1982). *Phys. Status Solidi A*, **69**, 483–490.

LITZMAN, O. & JANÁČEK, Z. (1974). *Phys. Status Solidi A*, **25**, 663–666.

NOURTIER, C. & TAUPIN, D. (1981). *J. Appl. Cryst.* **14**, 432–436.

PENNING, P. & POLDER, D. (1961). *Philips. Res. Rep.* **16**, 419–440.

SØRUM, H. & BREMER, J. (1980). *J. Appl. Cryst.* **13**, 359–363.

TAKAGI, S. (1969). *J. Phys. Soc. Jpn*, **26**, 1239–1253.

TAUPIN, D. (1964). *Bull. Soc. Fr. Minéral. Cristallogr.* **87**, 469–511.

URAGAMI, T. (1969). *J. Phys. Soc. Jpn*, **27**, 147–154.

WERNER, S. A. (1974). *J. Appl. Phys.* **45**, 3246–3254.

Acta Cryst. (1984). A**40**, 291–296

The Theory of the Pauling–Simon Law on Lattice Constants of Close-Packed Ordered Alloys

BY CLARE D. CHURCHER AND VOLKER HEINE

Cavendish Laboratory, Madingley Road, Cambridge CB3 0HE, England

(*Received* 29 *July* 1983; *accepted* 21 *December* 1983)

Abstract

In close-packed ordered alloys of composition AB_n the lattice constant a and all interatomic distances are determined to a good approximation by the quantity $(R_A + nR_B)$. This observation, the Pauling–Simon law [Pauling (1957). *Acta Cryst.* **10**, 374–375; Simon (1983). *Angew. Chem.* **22**, 95–113], is analogous to Vegard's law [Pearson (1972). *The Chemistry and Physics of Metals and Alloys.* New York: Wiley] for random alloys. No exact proof is possible but here a theoretical discussion is given using the spirit of Froyen & Herring's 'proof' of Vegard's law [Froyen & Herring (1981). *J. Appl. Phys.* **52**, 7165–7167]. The

0108-7673/84/030291-06$01.50